PHYSICAL REVIEW C VOLUME 19, NUMBER 3 MARCH 1979

Fusion and nonfusion processes in reactions induced by 10–100-MeV ^{6}Li ions with Fe targets

J. Jastrzębski
Indiana University Cyclotron Facility, Bloomington, Indiana 47401
and Institute for Nuclear Research, Swierk, Warsaw, Poland

H. Karwowski,† M. Sadler,‡ and P. P. Singh
Indiana University Cyclotron Facility, Bloomington, Indiana 47401
(Received 1 August 1978)

Excitation functions and projected recoil ranges for radioactive nuclei produced in the ^{6}Li bombardment of ^{54}Fe an ^{56}Fe targets over 10 to 100 MeV energy range have been measured using the activation technique. At 55 and 85 MeV differential ranges have also been measured for the ^{56}Fe target. Using the in-beam gamma-ray technique production cross sections for many residual nuclei were measured for the ^{6}Li + ^{56}Fe system for a ^{6}Li energy range of 55 to 99 MeV. Close to 90% of the optical model reaction cross section is observed over the entire energy range. About 80% of the observed cross section corresponds to statistical evaporation of the compound nucleus. Above about 30 MeV ^{6}Li energy ^{56}Fe(^{6}Li,α)^{58}Co* transfer process can explain the observed behavior of recoil ranges. It contributes about 300 mb to the production of various nuclei reached through evaporation decay of ^{58}Co*. Pre-equilibrium nucleon emission appears to be noticeable above 60 MeV and contributes 100 mb to the production process at 80 MeV. A reasonable account of the observed cross section for various product nuclei is given by the predictions of the fusion-evaporation model. In its fusion characteristics the ^{6}Li projectile appears to behave very much like other light heavy ions.

[NUCLEAR REACTIONS ^{54}Fe(^{6}Li, X), ^{56}Fe(^{6}Li, X), E=10–100 MeV. Measured $E\gamma$, $I\gamma$; deduced $\sigma(X,E)$, recoil ranges, σ transfer, σ pre-equilibrium nucleon emission, σ fusion, mass distribution. Enriched targets, Ge(Li) counting, in-beam gamma-ray and radioactivity techniques.]

I. INTRODUCTION

The motivation for this work was to use the higher energy lithium beams available from the Indiana University Cyclotron Facility to study the characteristics of the cross sections and patterns of momentum transfer to various nuclei produced in lithium induced reactions on medium mass nuclei at energies higher than had been studied before with the aim of determining the specific role of various reaction mechanisms that may be involved. Previous studies[1,2] for one of the systems studied here, ^{6}Li on ^{54}Fe, were confined to ^{6}Li energies of 15–60 MeV and were limited to measurements of long lived radioactive products which could be studied by activation techniques. The main conclusion concerning the reaction mechanism was that the dominant mechanism of production is the fusion of the projectile and the target nucleus, with formation of a compound nucleus that decays through statistical evaporation of nucleons and other particles. Some evidence concerning the role of direct one-nucleon transfer reactions in the production of neighboring nuclei such ^{55}Co and ^{55}Fe, and of pre-equilibrium nucleon emission, was noted.

In the present work we have measured production cross sections and integral recoil ranges of short and long lived radioactive nuclei by the activation technique over the ^{6}Li energy range of about 10 to 100 MeV for ^{54}Fe and ^{56}Fe targets, and have measured production cross sections for almost all nuclear products of ^{6}Li bombardment of ^{56}Fe in the energy range of 55 to 99 MeV using the in-beam γ technique. To obtain a detailed picture of the manner in which the incident momentum is transferred differential ranges were measured at 55 and 84 MeV. From the results of these measurements we have been able to identify the contributions of various reaction mechanisms and also to determine the extent to which various mechanisms are involved in the production of different final nuclei. Wherever possible we have limited ourselves to conclusions that can be drawn solely on the basis of the character and the magnitude of the measured quantities. Since the dominant mechanism appears to be fusion evaporation, comparisons of the measured cross section are made only with the predictions of such a model using the computer code ALICE.[3]

One of the objectives of this work was to compare and contrast the nuclear interaction mech-

anisms of ^{6}Li ions with those of other light heavy ions. It appears that ^{6}Li induced reactions may involve all the processes such as fusion, incomplete fusion, particle or cluster transfer, and pre-equilibrium nucleon and cluster (such as α-particles) emission that have been identified as playing a significant role in light heavy ion induced reactions. Further work is needed to determine whether the degrees of relative importance of these various processes are similar or different in the two cases.

II. EXPERIMENTAL METHODS AND RESULTS

A. Beam and targets

^{6}Li ions were accelerated in a three stage, variable energy accelerator system at the Indiana University Cyclotron Facility. Complete stripping of the ions was achieved before the beam entered the last acceleration stage. The extracted beam energy was determined with the help of an analyzing magnet, and was known to be within ±0.3 MeV.

The on-line γ-ray measurements (see Sec. II B) were performed using a beam of about 0.5 enA intensity incident upon targets about 3 mg/cm^2 thick in the low intensity target station. The transmitted beam was collected in a three-section Faraday cup and its total charge was measured using a calibrated charge integrator.

Samples for off-line residual radioactivity measurements (see Sec. II C) were produced using 10 to 50 enA of ^{6}Li beam in the hot cell radiation area. The target assemblies consisted of a stack of Fe foils (about 4 mg/cm^2) and Al or Kapton catchers, interspersed with Al beam energy degraders. Up to twelve new target-catcher combinations were used for each bombardment. The total beam energy degradation by the complete stack was about 50 MeV. A beam collimator, 5 mm in diameter, was placed upstream from the stack. An assembly of the stack and a downstream beam stopper, connected to the current integrator, was housed in a cage maintained at −500V to ensure complete charge collection.

Isotopically enriched ^{54}Fe and ^{56}Fe self-supporting targets were prepared from elemental powder by melting on an alumina coated strip and rolling in a pack of 304 stainless steel. The ^{56}Fe target contained less than 0.08% of other Fe isotopes and therefore no correction to the measured cross sections for other isotopes was necessary. Data obtained with the ^{54}Fe target (96.81% rich in ^{54}Fe) were corrected for a contribution from 3.04% of ^{56}Fe.

The thicknesses of all targets and catchers were determined by measuring the energy degradation of α particles from a ^{241}Am source and comparing it with the energy loss obtained from the tables of Ref. 4. The thickness of the targets was found to be uniform within 10%. The thin Al catchers used for the measurements of the differential recoil ranges (see Sec. II D) were selected to have a thickness which was uniform to better than 5%.

B. In-beam cross section determinations

In-beam γ-ray singles spectra resulting from the bombardment of the ^{56}Fe target with ^{6}Li ions were measured using a Ge(Li) detector having 10% efficiency and 2.5 keV energy resolution for 1.33-MeV γ rays. Most measurements were made with the Ge(Li) detector placed about 3 cm from the target and at 90° with respect to the beam. This geometry led to the lowest background contribution. Angular distribution effects were investigated at two bombarding energies by making additional measurements at 125° and were found to be insignificant.

For each bombarding energy γ-ray spectra were collected during 1–2 h at a rate of $2-4\times10^3$ counts per second. Absolute cross sections for the production of individual γ lines were determined after correction for dead time losses. γ-ray spectra recorded between beam bursts, and immediately after the bombardment, were used to estimate the radioactivity contributions to the individual γ-ray intensities. These corrections were found to be negligible for all but a few observed lines.

Attribution of the observed γ rays to a particular final nucleus was made on the basis of the measured energies and the consistency of relative intensity patterns with those observed or expected for that nucleus. For this purpose a list of γ rays assigned on the basis of in-beam measurements to nuclei with $45 \leq A \leq 62$ was prepared from the recently published literature. A summary of the observed γ rays and their assignments can be obtained from the authors.[5] From the cross sections determined for strong and well-resolved peaks in measurements performed under different conditions with respect to the beam intensity, and detector to target distance, systematic errors are estimated to be about 15%.

Cross sections for the production of individual final nuclei were obtained by summing observed cross sections for transitions leading to the ground state, or in some cases to low lying excited states when the corresponding transition to the ground state was not detected. Corrections for side feeding to the ground state were not attempted. Table I summarizes the production cross sections of final nuclei identified through the in-beam measurements for all bombarding energies used in this study.

TABLE I. Cross sections (in mb) for ^{6}Li + ^{56}Fe reaction products determined from the in-beam γ-ray measurements.

Product	E_{lab} (MeV) 55.2	65.0	77.6	84.1	91.4	97.0	99.1
^{59}Ni	43	15	22	8		4	4
^{58}Ni	58	29		11	12	4	4
^{57}Ni				7		6	
^{59}Co	32	50		13		26	29
^{58}Co	252	155	119	99	63	61	53
^{57}Co	a						
^{56}Co	70	63	90	97	86	72	79
^{58}Fe	≃8 [b]			≃6		≃6	
^{57}Fe	99	98	145	113	87	97	94
^{56}Fe	211	195	308	283	242	270	280
^{55}Fe	204	152	153	181		187	198
^{54}Fe	17	30	30	72		63	58
^{53}Fe	6	6		7		20	
^{55}Mn	47	43	48	43	42	46	47
^{54}Mn	57	110	183	168	122	129	119
^{53}Mn	10	16	69	115		136	126
^{52}Mn	23	27	24	34	24	31	45
^{51}Mn	6	7	15	11	10	7	13
^{54}Cr				24 [c]		27	17
^{53}Cr	≃20 [d]	≃3		≃24		≃33	≃27
^{52}Cr	19	13	40	34	39	66	58
^{51}Cr				53		62	
^{50}Cr				17		33	30
^{51}V				4 [e]		4	
^{50}V				8		9	12
^{49}V				12		26	25
^{47}V				2		3	4
^{48}Ti				7		11	9

[a] Production cross section for ^{57}Co could not be estimated since there was no satisfactory way to determine the exact contribution of the intense 1222.8-keV ^{55}Fe transition to the 1223.6-keV peak.

[b] Contribution of the overlapping $2^+ \rightarrow 3^+$ transition of ^{56}Co to the 810.6-keV peak (see Table I) was estimated from the observed intensities of other transitions of ^{56}Co.

[c] Since the γ peak corresponds to $2^+ \rightarrow 0^+$ transition overlaps with the $\frac{13}{2}^- \rightarrow \frac{11}{2}^-$ transition in ^{57}Co (see Table I), the production cross section for ^{54}Cr is assumed to be 1.7 times the cross section for its $4^+ \rightarrow 2^+$ transition. The factor 1.7 is based upon the corresponding systematics of other even-even nuclei.

[d] Contribution of the ^{58}Ni $4^+ \rightarrow 2^+$ transition to the 1005.1-keV peak was estimated using the observed intensity of its $2^+ \rightarrow 0^+$ transition.

[e] Based only upon the $\frac{11}{2}^-$ to $\frac{7}{2}^-$ 1609.3-keV peak.

C. Cross sections determined from residual radioactivity

γ-ray spectra from irradiated ^{54}Fe and ^{56}Fe targets and the associated Al or Kapton catchers were recorded alternately beginning about 10 minutes after the end of the bombardment and during the following 3 months. A Ge(Li) counter with 1.8-keV energy resolution and 10% efficiency, placed in lead shielding, was used for these measurements. Half-lives, energies, and branching ratios were taken from Ref. 6. The total production cross section of a given reaction product was obtained by summing the cross sections determined separately from target and catcher activities. For each but the shortest lived products at least four independent activity measurements were made. Average values of the cross sections so determined are presented in Tables II and III and are plotted in Figs. 1 and 2. The quoted errors were estimated from the spread in the values of the cross section obtained through different measurements for all relevant transitions.

D. Recoil ranges of the radioactive reaction products

Integral recoil ranges, projected on the beam direction, were determined using the measurements described in the previous section. Ranges were obtained from the relation $R = WA_c/(A_c + A_t)$ where W is the target thickness and A_c and A_t are the activities of a given reaction product observed in the catcher and target foils respectively. The results of these measurements are presented in Tables IV and V and in the lower parts of Figs. 1 and 2.

Differential recoil ranges (thin target) were determined at bombarding energies of 55 and 84 MeV. Up to eight Al catchers, about 200 μg/cm^2 thick, were used. The analysis of the experimental data follows closely previous works in this field.[7,8] The thin target data are summarized in Table VI and are also illustrated in Fig. 3.

A comparison of the projected average recoil ranges in Al, for those cases which exhibit a symmetric distribution (see Fig. 3), with corresponding ranges in Fe, has been made with the help of the range-energy tables.[4] This comparison shows that the ranges in Al are systematically about 10% higher than those in Fe. Although this difference may still be within the precision of the tabulated range-energy relationships, we believe that it is a real effect originating from multiple scattering of the recoiling ions.

The scattering correction for slowly recoiling ions was developed by Lindhard and Scharff.[9] This correction may be written approximately as

$$R \approx R_{meas}\left(1 + \frac{M_t}{xM_R}\right),$$

where R_{meas} and R are measured (projected) and true ranges, respectively, M_t and M_R are the masses of the target atoms and recoiling ions, respectively, and x is a coefficient, calculated by

TABLE II. Cross sections (in mb) for $^{6}Li + ^{56}Fe$ reaction products determined from the radioactivity measurements.

Product	E_{lab} (MeV) 15.4	21.1	29.3	33.7	41.6	46.8	53.5	56.5	64.3	72.0	84.0	95.1
^{61}Cu		0.8 (3)		0.3 (1)								
^{60}Cu	55 (15)	54 (5)	19 (4)	8.7(15)								
^{57}Ni						1.2 (2)	3.9 (6)	5.0 (5)	9.5(10)	11.7 (6)	7.2 (3)	5.2 (8)
^{60}Co	15 (5)	27 (4)	8 (5)									
$^{58}Co^{m+g}$	2.8 (3)	6.2 (5)	37 (3)	117 (8)	335 (15)	498 (30)	402 (15)	350 (15)	262 (8)	185 (8)	85 (3)	57 (5)
^{57}Co	233 (15)	303 (20)	210 (10)	169 (12)	135 (8)	172 (12)	259 (10)	258 (15)	403 (20)	403 (20)	251 (10)	215 (15)
^{56}Co	1.0 (5)	4.2 (5)	64 (3)	91 (9)	105 (5)	101 (8)	81 (6)	75 (5)	81 (5)	98 (12)	105 (5)	104 (7)
^{55}Co				0.2 (1)	4.5 (7)	9.5 (6)	12 (2)	11 (2)	10 (1)	9.8 (5)	8.2 (5)	11.7 (7)
^{59}Fe				1.0 (3)		1.6 (3)						
^{56}Mn			1.1 (3)	2.1 (3)	6.1 (3)	6.4 (5)	6.7(10)	5.2 (5)	5.7 (6)	6.7 (6)	6.0 (3)	9.5 (5)
^{54}Mn	7 (2)	15 (2)	24 (2)	24 (2)	18 (2)	24 (2)	39 (4)	57 (5)	146 (10)	229 (13)	170 (8)	145 (8)
$^{52}Mn^{g}$					1.5 (2)	9 (1)	20 (1)	21 (1)	23 (1)	21 (2)	20 (1)	40 (1)
$^{52}Mn^{m}$						0.9 (2)		3 (1)		2.4 (6)		
^{51}Cr								5 (2)	36 (2)	80 (5)	74 (3)	76 (3)
^{48}V										2.5 (3)	5.0 (2)	5.3 (8)

TABLE III. Cross sections (in mb) for $^{6}Li + ^{54}Fe$ reaction products determined from the radioactivity measurements.

Product	E_{lab} (MeV) 9.8	16.8	25.6	30.9	39.0	44.6	51.4	55.5	62.4	70.4	83.0	94.0
^{57}Ni	0.4(2)	11 (1)	55 (5)	79 (5)	61 (5)	34 (4)	15 (2)	12 (2)	7.7(8)	4.7(4)	2.6 (7)	1.5 (5)
^{56}Ni			0.12 (6)	0.47(12)	2.1 (3)	3.2 (4)	3.4 (5)	3.1 (8)	2.6(4)	1.9(5)	1.3 (2)	1.1 (5)
$^{58}Co^{m+g}$ [a]	5 (1)	116 (8)	79 (5)	53 (7)	24 (5)	16 (4)			6 (1)	3 (1)	2.3 (8)	1.8 (8)
^{57}Co [a,b]	5 (1)	122 (10)	555 (30)	658 (40)	419 (30)	274 (30)	112 (15)	79 (10)	54 (8)	31 (6)	14 (4)	9 (3)
^{56}Co			11 (2)	39 (2)	177 (9)	263 (27)	212 (18)	220 (18)	149 (7)	99 (7)	62 (2)	47 (7)
^{55}Co	13 (2)	84 (5)	75 (4)	76 (6)	51 (4)	51 (4)	48 (5)	46 (5)	59 (4)	71 (4)	49 (4)	45 (5)
^{52}Fe								0.3 (2)	2 (1)	3.6(3)	4.4 (2)	4.8 (4)
^{54}Mn			43 (4)	97 (5)	142 (10)	140 (10)	74 (10)	86 (8)	86 (7)	122 (6)	144 (10)	132 (8)
$^{52}Mn^{g}$		1.9 (3)	10 (1)	13.7 (6)	10 (1)	11 (2)	17 (1)	27 (2)	94 (2)	176 (7)	149 (5)	118 (6)
$^{52}Mn^{m}$		2.6 (3)		8 (1)		2.1 (4)				17 (4)		
^{51}Cr			3 (2)	15 (2)	47 (3)	67 (5)	50 (5)	51 (3)	56 (3)	97 (4)	190 (20)	250 (10)
^{49}Cr										11 (2)		30 (10)
^{48}Cr												1.5 (5)
^{48}V						1.4 (2)		2.1 (5)		4.0(4)	21 (2)	44 (4)

[a] Quoted cross sections are corrected for ^{56}Fe isotope, present in ^{54}Fe target.
[b] Quoted cross sections are independent.

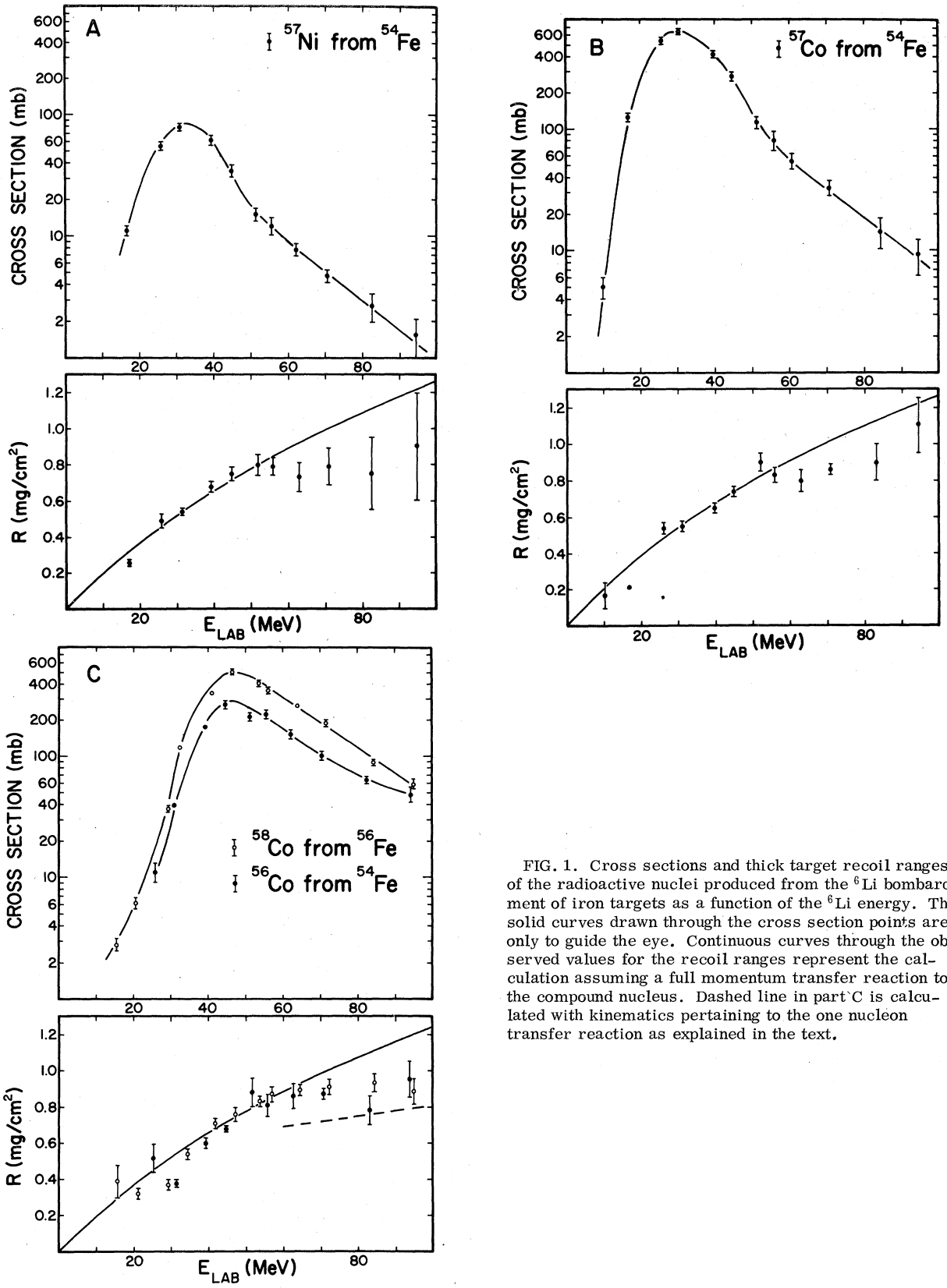

FIG. 1. Cross sections and thick target recoil ranges of the radioactive nuclei produced from the ^{6}Li bombardment of iron targets as a function of the ^{6}Li energy. The solid curves drawn through the cross section points are only to guide the eye. Continuous curves through the observed values for the recoil ranges represent the calculation assuming a full momentum transfer reaction to the compound nucleus. Dashed line in part C is calculated with kinematics pertaining to the one nucleon transfer reaction as explained in the text.

Lindhard and Scharff to have the value of 3 for slow ions. Empirically, in the recoiling energy range of importance here, a slightly better agreement between the calculated and the measured ranges and between Al and Fe data is obtained with $x = 5$. The solid lines drawn in the lower parts of Figs. 1 and 2 represent the ranges calculated assuming full momentum transfer and the scattering correction with $x = 5$. The better agreement obtained with $x = 5$ instead of $x = 3$ may perhaps be explained by the fact that, in the calculated ranges, we did not take into account a small increase in the recoil range of the compound nucleus due to nucleon evaporation.[7]

E. Cross section distribution for ^{56}Fe target

The distribution of cross section for production of various nuclei, determined with a target of ^{56}Fe through in-beam and residual activity measurements, is displayed in Fig. 4 for 55- and 100-MeV ^{6}Li bombarding energy. Since the in-beam and the activity measurements were not made at exactly the same energies, some of the cross sections indicated in Fig. 4 were obtained by interpolation.

The total observed cross sections for the ^{56}Fe target in the energy range of 50 to 100 MeV are presented in Fig. 5. Figure 6 shows the mass distribution for three different excitation energies of the compound system, and in Fig. 7 the mean number of nucleons emitted from the compound nucleus is plotted vs excitation energy.

III. DISCUSSION

A. Reaction mechanism

A glance at the pattern of the observed production cross section among various nuclei as displayed in periodic chartlike tables of Fig. 4 reveals that nuclei closer to the line of stability are in general produced with larger cross sections. This pattern is very characteristic of the fusion-evaporation process. Indeed as will be shown in this section all but about 20% of the observed reaction cross section is consistent with this mechanism. The role and nature of other mechanisms in the production of various final nuclei is deciphered from the character of the individual excitation functions and that of the results on integral and differential ranges as discussed below.

Product nuclei with $A \geq A_{\text{target}} + 2$ *and* $Z \geq Z_{\text{target}} + 1$. The production of the nuclei in this group is exemplified by the excitation functions and recoil ranges of ^{56}Co, ^{57}Co, ^{57}Ni (from ^{54}Fe target) and ^{58}Co (from ^{56}Fe target) shown in Fig. 1. Their excitation functions are characterized by a broad peak which is typical of the process in which the target and the projectile have fused to form a compound nucleus at high excitation which in turn decays by nucleon evaporation producing a broad range of final products. This characterization is supported by the measured integral recoil ranges whose values are consistent with those calculated (solid curves in Fig. 1) on the assumption that the full momentum of the incident projectile is transferred to the compound nucleus. Beyond about 20 MeV above the energy of the peak, the excitation functions exhibit an exponential tail and the recoil ranges level off to values below those for full-momentum transfer. The exponential tail shows the onset of higher energy nucleon emission during the pre-equilibrium phase of the nuclear reaction. The effect of emission of one pre-equilibrium nucleon on the recoil ranges can be estimated since it is kinematically equivalent to a transfer reaction of the type $A(^{6}\text{Li}, n)B^{*}$. The dashed line in Fig. 1 represents the values of the recoil ranges using the recoil energies of ^{61} Cu* produced at an excitation of 50 MeV in a grazing-angle peaked $^{56}\text{Fe}(^{6}\text{Li}, n)^{61}\text{Cu}^{*}$ reaction. The 50-MeV excitation of ^{61}Cu is deemed necessary to produce ^{58}Co at an average excitation of 8 MeV after evaporating a neutron and two protons with an average kinetic energies of 3.5 and 7 MeV, respectively. It is obvious that a contribution from pre-equilibrium nucleon emission will tend to level off the recoil range to a value below the full momentum value. Using the method and the arguments described below, the contribution of the process involving emission of a pre-equilibrium nucleon is estimated to be 130 ± 30 mb at 80-MeV ^{6}Li energy.

Product nuclei with $A < A_{\text{target}} + 2$ *and* $Z \leq Z_{\text{target}} + 1$. Such nuclei typically show a double humped excitation function and a similar behavior for their recoil ranges as shown in Fig. 2 for ^{57}Co, ^{56}Co, ^{55}Co, ^{56}Mn, and ^{54}Mn produced from the ^{56}Fe target and for ^{55}Co, ^{54}Mn, and ^{52}Mn produced with the ^{54}Fe target. The position of the peaks in the excitation functions can be understood in terms of the fusion-evaporation model. For example, the positions of the first peak in the excitation functions of Figs. 2(A)–2(C) are within 5 MeV of those expected for the process involving one α evaporation from the compound nucleus, while the position of the second peak is consistent with that involving nucleon evaporation only. In the cases of Fig. 2(E) the positions of the two peaks can be explained in terms of statistical emissions including two and one α particles, respectively. In the fusion-evaporation model the positions of the peaks in the cross sections are close to those calculated by assuming that mean kinetic energies of the evaporated neutron, proton, and α particle are 3.5, 7, and 13 MeV, respectively, and that the mean exci-

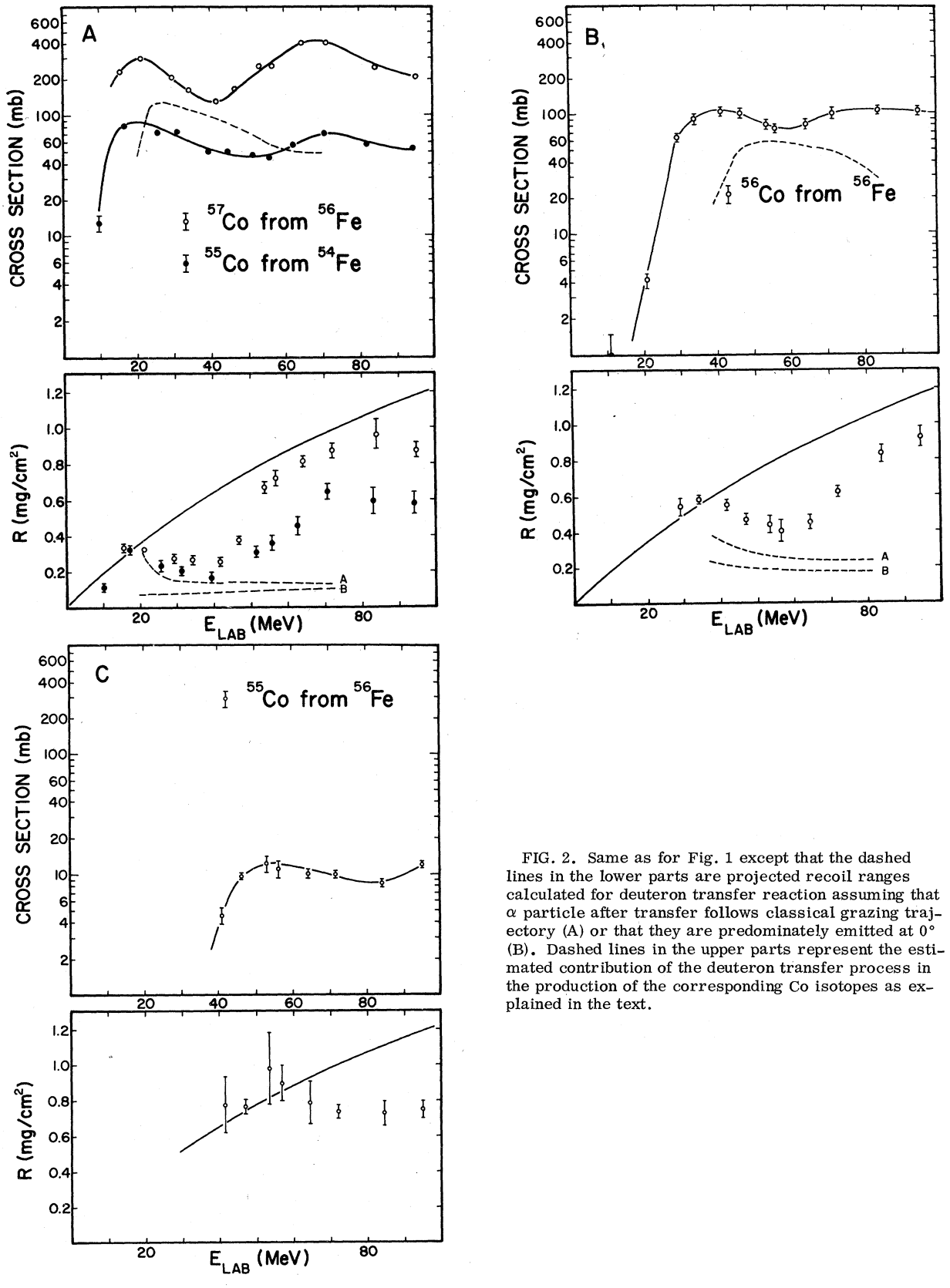

FIG. 2. Same as for Fig. 1 except that the dashed lines in the lower parts are projected recoil ranges calculated for deuteron transfer reaction assuming that α particle after transfer follows classical grazing trajectory (A) or that they are predominately emitted at 0° (B). Dashed lines in the upper parts represent the estimated contribution of the deuteron transfer process in the production of the corresponding Co isotopes as explained in the text.

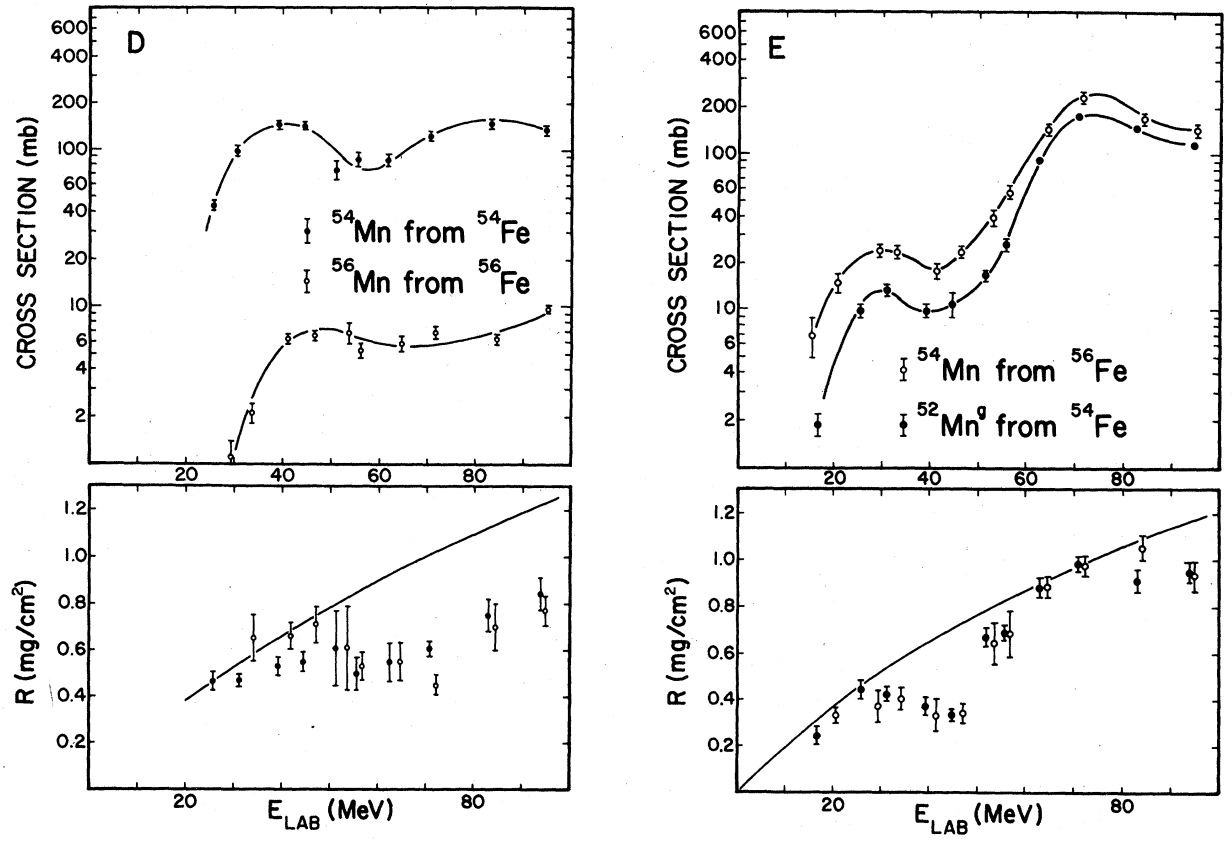

FIG. 2. (*Continued*)

tation of the residual final nucleus is 8 MeV. As presented in a subsequent section, the statistical model is able to explain not only the shapes of the observed excitation functions but also the magnitude of the cross sections for most product nuclei.

The behavior of the integral recoil ranges with bombarding energy cannot be understood in terms of the fusion-evaporation picture alone. Whereas up to the first peak in the excitation functions the measured ranges are consistent with values corresponding to full momentum transfer, the drop in their values leading to well defined valleys and the eventual rise towards full momentum values at higher energies is a strong indication that there is a significant contribution of some other process, which transfers considerably less than the full incident momentum to the reaction products, in the ^{6}Li energy range above the first peak in the excitation functions. One cannot ascribe this behavior to evaporation of nucleons and/or α particles because, due to the isotropic nature of such emissions, evaporation does not significantly change the average value of the recoil ranges from the full momentum values. Striking evidence against the fusion-evaporation model being the sole process is provided by asymmetric behavior of the differential ranges (see Fig. 3) for ^{56}Co and ^{56}Mn at 55-MeV bombarding energy. Asymmetry implies contribution of a process producing recoil ranges of considerably smaller average value. Indeed in varying degree some asymmetry in the differential ranges is observed for all but ^{58}Co. Absence of asymmetry even in the 84-MeV differential ranges for ^{58}Co is consistent with the fact that the process responsible for the exponential tail in its excitation function is pre-equilibrium nucleon emission which does not substantially decrease the recoil ranges.

Possible mechanisms which could account for the lowering of the integral recoil ranges are (i) pre-equilibrium nucleon emission, (ii) direct (^{6}Li, α) and (^{6}Li, d) transfer reactions, (iii) break-up of ^{6}Li ions into α and d with subsequent capture of one of the fragments by the target nucleus, and (iv) a preferred emission of high energy α particles in the forward direction from the projectile plus target system prior to the establishment of statistical equilibrium.

One can easily rule out pre-equilibrium nucleon emission as being responsible for the observed character of the recoil ranges at these energies, since it at best can reduce the recoil ranges to

TABLE IV. Integral recoil ranges (in mg/cm^2 in ^{56}Fe) for ^{6}Li + ^{56}Fe reaction products.

Product	E_{lab} (MeV) 15.4	21.1	29.3	33.7	41.6	46.8	53.5	56.5	64.3	72.0	84.0	95.1
^{60}Cu		0.47(7)										
^{57}Ni						0.67(8)	0.97(23)	0.95 (9)	0.94(13)	0.99(4)	0.97 (7)	1.11(10)
^{58}Co^{m+g}	0.39(9)	0.32(3)	0.37(3)	0.54 (3)	0.71 (3)	0.76(4)	0.83 (3)	0.87 (4)	0.89 (3)	0.91(4)	0.93 (5)	0.88 (7)
^{57}Co	0.34(2)	0.33(1)	0.28(2)	0.27 (2)	0.26 (2)	0.38(2)	0.67 (3)	0.72 (4)	0.81 (3)	0.87(4)	0.96 (8)	0.87 (4)
^{56}Co			0.54(5)	0.58 (2)	0.55 (3)	0.47(3)	0.44 (5)	0.40 (6)	0.45 (4)	0.62(3)	0.83 (5)	0.92 (6)
^{55}Co					0.78(16)	0.77(4)	0.98(20)	0.90(10)	0.79(12)	0.74(4)	0.73 (7)	0.75 (5)
^{59}Fe				0.7 (2)		0.7 (2)						
^{56}Mn				0.65(10)	0.66 (6)	0.71(8)	0.61(18)	0.53 (6)	0.55 (8)	0.45(4)	0.70(10)	0.77 (6)
^{54}Mn	0.5 (2)	0.34(3)	0.38(7)	0.41 (5)	0.34 (7)	0.35(4)	0.65 (9)	0.69(10)	0.89 (4)	0.98(4)	1.06 (5)	0.94 (6)
^{52}Mn^g					0.71(12)	0.72(4)	0.98 (5)	0.95 (5)	0.97 (8)	0.93(5)	0.87 (7)	1.08 (4)
^{51}Cr									1.00 (8)	1.05(5)	1.1 (1)	1.13 (8)
^{48}V											1.05(15)	1.23 (5)

about 80% of the full momentum value, as indicated previously; the lowest observed values of the recoil ranges from the ^{56}Fe target are a factor of 2, for ^{56}Co and ^{56}Mn, and three, for ^{57}Co, smaller than the full momentum values at the corresponding energies.

In a transfer reaction such as (^{6}Li, α) the outgoing α particle can carry away a significant part of the incident momentum since cross sections for these reactions are established to be peaked slightly forward of the classical grazing angle (which lies between 30° to 10° for the ^{6}Li + ^{56}Fe system over 30- to 90-MeV ^{6}Li energies). In this case one visualizes that, e.g., ^{58}Co is left at an excitation energy higher than the particle emission threshold following the ^{56}Fe(^{6}Li, α)^{58}Co* reaction, from where it decays by evaporation of one or more nucleons depending upon its excitation energy. The cross section for the transfer reaction is expected to peak around an optimum-Q value, which for this case varies from about 15 to 50 MeV in ^{58}Co for ^{6}Li energies of 20 to 100 MeV. Thus the maximum contribution of the transfer process would shift from $A = 57$ product nuclei at around 30-MeV ^{6}Li energy to $A = 56$ nuclei at about 60 MeV, corresponding to evaporation of one and two nucleons from ^{58}Co*, respectively. This is consistent with the energies where we see the lowest ranges for ^{57}Co and ^{56}Co product nuclei [see Figs. 2(A) and 2(B)]. Further, since the excitation of ^{58}Co increases smoothly with ^{6}Li energy, the contribution of the transfer reaction to any specific final nucleus, such as ^{57}Co, would gradually increase to a maximum value and then decrease slowly, which makes this process capable of explaining the qualitative features of the observed behavior of the recoil ranges for a given product nucleus with the ^{6}Li energy.

The dashed lines labeled A and B in Figs. 2(A) and 2(B) represent the recoil ranges of ^{58}Co* left at excitation energies of 20 and 35 MeV, the optimum excitation energies to evaporate one and two neutrons from ^{58}Co* to produce ^{57}Co and ^{56}Co, respectively, following the ^{56}Fe(^{6}Li, α)^{58}Co* reaction. Curve A corresponds to the transfer reaction peaking at the grazing angle and curve B corresponds to peaking at 0°. The recoil energies of ^{58}Co were calculated kinematically for the above conditions and the projected ranges were obtained using the range-energy tables of Northcliffe and

TABLE V. Integral recoil ranges (in mg/cm^2 in ^{54}Fe) for ^{6}Li + ^{54}Fe reaction products.

Product	E_{lab} (MeV) 9.8	16.8	25.6	30.9	39.0	44.6	51.4	55.5	62.4	70.4	83.0	94.0
^{57}Ni		0.26(2)	0.49(4)	0.54(2)	0.69(3)	0.75(4)	0.80 (6)	0.79 (5)	0.73(8)	0.79(10)	0.75(20)	0.9 (3)
^{56}Ni				0.42(9)	0.58(6)	0.68(3)		0.81(12)	0.81(7)	0.85(10)	0.75(15)	
^{58}Co^{m+g}		0.28(2)	0.61(3)	0.61(5)	0.68(7)	0.76(6)	0.88(12)		0.89(9)	0.99 (7)	0.8 (3)	
^{57}Co	0.17(7)	0.21(1)	0.54(3)	0.55(3)	0.65(3)	0.74(3)	0.90 (5)	0.83 (5)	0.80(6)	0.86 (3)	0.9 (1)	1.11(16)
^{56}Co			0.52(8)	0.38(2)	0.60(3)	0.68(2)	0.88 (8)	0.81 (6)	0.86(7)	0.87 (3)	0.78 (8)	0.95(10)
^{55}Co	0.12(2)	0.33(2)	0.24(3)	0.21(2)	0.17(3)	0.17(1)	0.31 (3)	0.36 (4)	0.45(5)	0.64 (4)	0.59 (7)	0.58 (6)
^{52}Fe										0.93 (4)	0.83(10)	0.80 (5)
^{54}Mn			0.47(4)	0.47(3)	0.53(4)	0.55(4)	0.61(16)	0.50 (7)	0.55(8)	0.61 (3)	0.75 (7)	0.84 (7)
^{52}Mn^g		0.25(4)	0.45(4)	0.43(3)	0.38(4)	0.35(2)	0.68 (4)	0.70 (3)	0.89(4)	0.99 (3)	0.92 (5)	0.96 (4)
^{51}Cr				0.46(4)	0.59(6)	0.64(3)	0.81(17)	0.65(10)	0.59(7)	0.73 (4)	0.89 (7)	1.01 (4)
^{48}V						0.73(7)		0.9 (3)		0.85 (4)	0.95(10)	1.11 (4)

TABLE VI. Summary of the differential recoil range data for the reaction $^{6}Li + ^{56}Fe$.

Bombarding energy (MeV)	Target thickness (mg/cm^2)	Reaction product	$R0$ average range in Al in mg/cm^2 [a]	Rm median range in Al in mg/cm^2 [b]	ρ straggling parameter a
84	0.459	^{58}Co	0.636	0.630	0.48
		^{57}Co	0.653	0.650	0.62
		^{56}Co	0.595	0.60	
		^{55}Co	0.511	0.47	
		^{56}Mn	0.514	0.46	
		^{54}Mn	0.724	0.710	0.65
		^{52}Mn	0.702	0.680	0.73
		^{51}Cr	0.762	0.750	0.55
55	0.276	^{58}Co	0.572	0.570	0.40
		^{57}Co	0.497	0.52	0.65 [c]
		^{56}Co	0.33		
		^{56}Mn	0.42		
		^{52}Mn	0.631	0.620	0.57

[a] See Ref. 8 for definition.
[b] Calculated from the probability plot.
[c] From the slope on the probability plot at 50% of the activity transmitted.

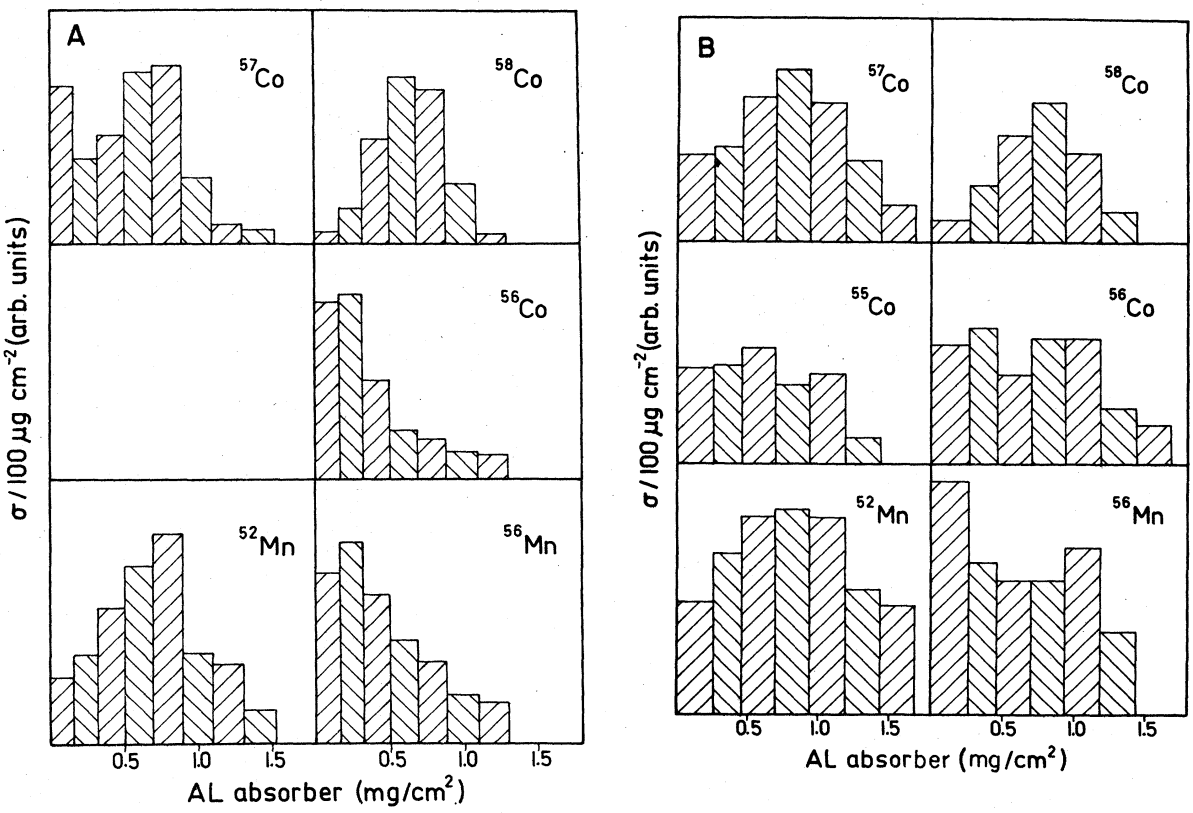

FIG. 3. Thin target differential recoil ranges for Co and Mn isotopes observed in $^{6}Li + ^{56}Fe$ reaction at 55-MeV (A) and 85-MeV (B) bombarding energies.

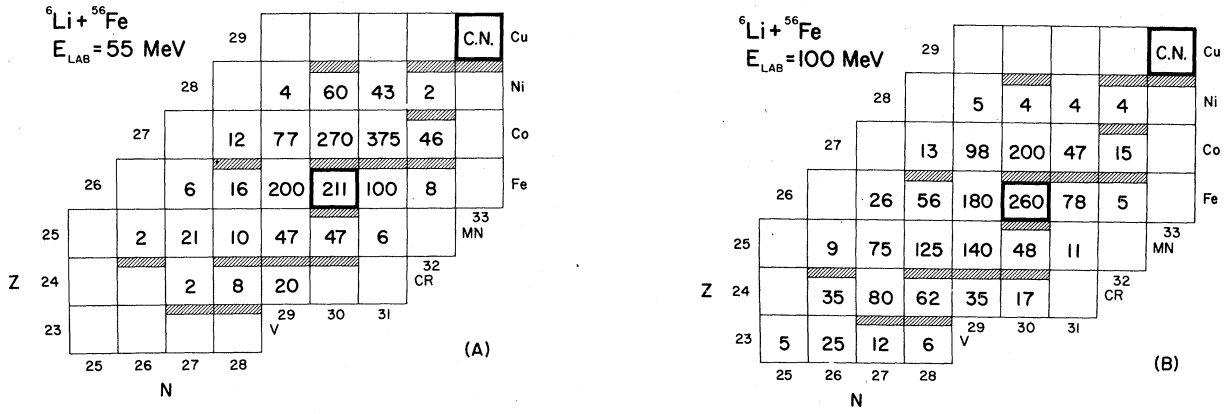

FIG. 4. Distribution of products from ^{6}Li+ ^{56}Fe reaction at 55-MeV (A) and 100-MeV (B) bombarding energies. Values of the cross section (in mb) were obtained from a smooth interpolation of the measured excitation function of each reaction product. In cases when both activation and in-beam values were available the cross sections determined by the activation measurements are shown.

Schilling.[4] It is obvious that a contribution from the (^{6}Li, α) reaction can reduce the ranges from the full momentum value to the observed values. The contribution of the (^{6}Li, α) reaction which will lead to the observed values of ranges can be quantitatively deduced using the relation

$$R_{\text{measured}} = kR_{\text{transfer}} + (1-k)R_{\text{full momentum}} .$$

Here $k = \sigma_{\text{transfer}}/\sigma_{\text{total}}$ and R with various subscripts represent the corresponding values of integral ranges. In the upper part of Figs. 2(B) and 2(C) the dashed curves represent the contribution of the transfer process computed in the manner outlined above, using R_{transfer} as the averages of

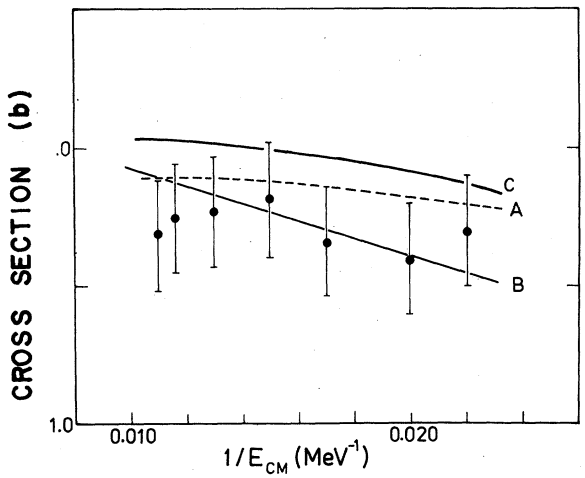

FIG. 5. Comparison of the total observed cross sections with the theoretical reaction cross section. Values for curve A are based upon the parabolic model (Ref. 15) and were obtained using a subroutine in ALICE (Ref. 3). Curve B represents the geometrical model for which $\sigma_R = \pi R^2(1 - Vc/E_{c.m.})$, where $R = 1.5(A_1^{1/3}+A_2^{1/3})$ fm and V_c is the relevant Coulomb barrier. The values predicted by the optical model (Ref. 16) are plotted as curve C. Values of the optical model parameters are V_r = 94.02 MeV, R_r = 1.304 fm, a_r = 0.820 fm, W = 23.75 MeV, R_i = 1.675 fm, and a_i = 0.778 fm and were found (Ref. 18) to give a reasonable account of the elastic ^{6}Li scattering in this energy range.

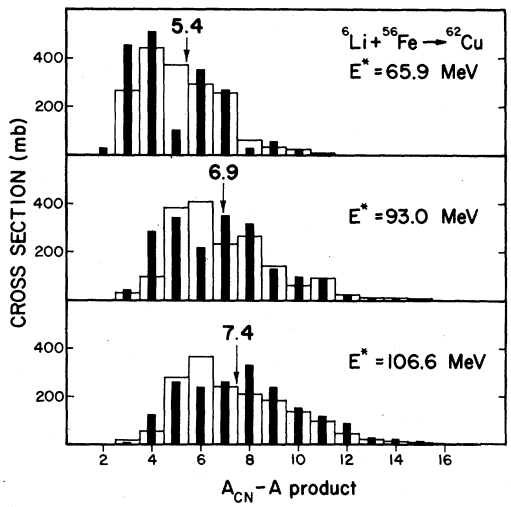

FIG. 6. Mass distribution of the reaction products from the ^{6}Li+ ^{56}Fe reaction. The arrows indicate the average "evaporated" mass for each excitation energy of the compound ^{62}Cu nucleus. The results of the fusion-evaporation model, obtained with code ALICE with options listed in Table VIII, as indicated by solid bars.

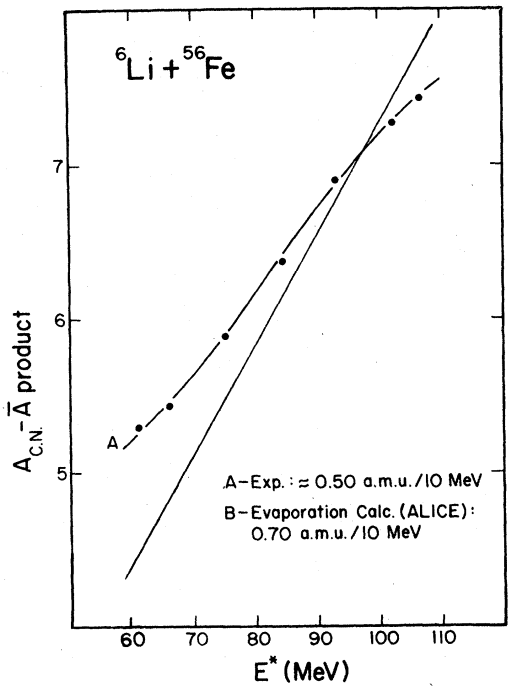

FIG. 7. Average "evaporated" mass (A) vs the excitation energy of the ^{62}Cu compound nucleus formed in the ^{6}Li + ^{56}Fe reaction. Solid line without points represents the results based upon the fusion-evaporation model.

the two values represented by curves *A* and *B* in the lower part of the figures at each energy. The shapes of the cross section contributed by the transfer reaction to the production of ^{57}Co and ^{56}Co are similar to each other and are shifted in energy by an amount expected for nuclei differing in mass by one unit and produced through evaporation from a common compound nucleus (^{58}Co in this case).

The total contribution of the *d*-transfer reaction can be estimated at any energy by summing the contributions to various product nuclei. For example, at 50-MeV ^{6}Li energy, ^{58}Co*, produced in the (^{6}Li, α) reaction, predominantly decays to nuclei of mass 56 and 57 via nucleon evaporation, and somewhat less probably to nuclei of mass 54 and 53 following α evaporation. The estimated contribution to the production of ^{57}Co and ^{56}Co nuclei at this energy is 131 ± 20 mb and for ^{54}Mn is 10 ± 3 mb [see Figs. 2(A) and 2(B)]. Since ^{53}Mn and ^{56}Mn are observed to be produced with a total cross section of less than 10 mb, the contribution to their production by the transfer process can be neglected. Assuming that ^{57}Fe and ^{56}Fe are produced by the transfer process with the same cross section as has been estimated for the corresponding cobalt nuclei, the total contribution of the transfer reaction amounts to 270 ± 40 mb. The estimated cross section for the transfer process does not appear to vary substantially above 35-MeV ^{6}Li energy.

In terms of the contributions made by the (^{6}Li, α) reaction one can also understand some differences in the behavior of the integral recoil ranges for the cases depicted in Figs. 2(A) to 2(D). Systematically lower ranges observed for ^{55}Co from the ^{54}Fe target as compared to those for ^{57}Co from the ^{56}Fe, in spite of the fact both are the same number of nucleons removed from the corresponding compound nuclei, represent the fact that ^{55}Co is produced with a lower cross section in the evaporation chain because it is relatively farther from the line of stability. In other words, relative contribution of the transfer reaction is higher for the ^{55}Co case than that for the ^{57}Co case.

Similarly, the near identity of the observed ranges for ^{56}Mn and ^{56}Co with an ^{56}Fe target, in spite of the fact that the total production cross section for ^{56}Mn is an order of magnitude smaller than that for ^{56}Co, implies that the relative ratio of the transfer and the fusion-evaporation processes is the same in the two cases. This is reasonable because for both processes evaporation of two additional protons would be inhibited in a similar way. Finally, it is interesting to note that the dip in the recoil ranges at 50 MeV observed for the ^{54}Mn (^{52}Mn) case(s) depicted in Fig. 2(E) corresponds to, and is energetically consistent with, the production of these nuclei after α evaporation from the transfer produced ^{58}Co*(^{56}Co*). The observed values of the recoil ranges for these nuclei at 50 MeV is consistent with a contribution of 10 mb by the transfer process to their production. The (^{6}Li, α) reaction could contribute to the production of ^{58}Co from the ^{56}Fe target but only in the range of 10–20 MeV ^{6}Li energy. Some evidence of a slight contribution may be present as the observed ranges are a bit smaller than the full momentum values.

The fact that the contribution, of about 300 mb in the total cross section, from the (^{6}Li, α) type transfer reaction can explain so many of the observed features of the integral recoil ranges which could not be understood in terms of the fusion-evaporation picture points to the inherent consistency of this picture and towards the credibility of its presence.

The role of the (^{6}Li, *d*) reaction to the production of various nuclei, in the same spirit as we discussed that for the (^{6}Li, α) reaction, is not so easy to establish. From the energetics its contribution can be expected to be largest around ^{6}Li bombarding energies of 37 MeV for $A = 58$, 52 MeV for $A = 57$, and 67 MeV from $A = 56$ product nuclei following nucleon evaporation from the excited ^{60}Ni

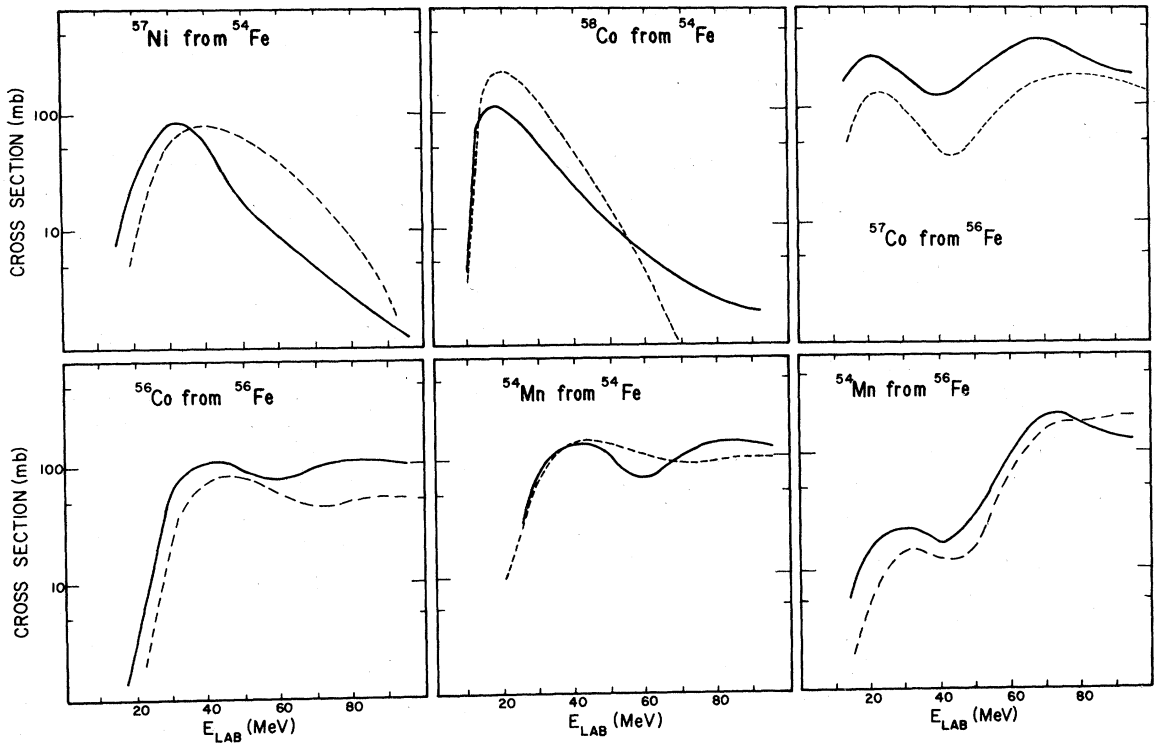

FIG. 8. Comparison of experimental (continuous curves) and calculated (dashed curves) excitation functions for the nuclei produced in the ^{6}Li+^{54}Fe and ^{6}Li+^{56}Fe reactions. The calculated values were obtained using the code ALICE with options listed in Table VIII.

nucleus produced in the ^{56}Fe(^{6}Li, d)^{60}Ni* reaction. The recoil energies and resulting ranges due to this process are a factor of 2 to 3 higher than that for the (^{6}Li, α) process under similar conditions. This rules out this process as the sole cause of lowest observed ranges for the cases shown in Figs. 2(A) to 2(D). However, some contribution from this process cannot be ruled out, especially 10–20 MeV above the minimum in the recoil ranges. Unfortunately there does not appear to be a distinctive characteristic in the observed ranges or the excitation functions from which one can deduce its contribution explicitly in a quantitative manner. The total contribution estimated above for the transfer reaction should, therefore, be considered to represent the combined total for (^{6}Li, α) and (^{6}Li, d) reactions though by far the larger contributions come from the former reaction.

It is interesting to note that effects in the recoil ranges similar to those reported here have also been seen with reactions induced by ^{11}B projectiles[10,11] on ^{109}Ag and ^{181}Ta targets. In these cases the role of reactions in which the complement of

TABLE VII. Input parameters used for the evaporation calculations (ALICE code, Ref. 3).

Inverse cross sections:	Calculated from the optical model subroutines incorporated in the code
Masses:	Myers Świątecki Lysekil masses Liquid drop masses Zero pairing
Type of calculation:	S wave approximation with rotating liquid drop moment of inertia at equilibrium deformation Parabolic barrier approximation for the reaction cross section No fission competition All partial waves included

the α particle for each projectile is transferred was conjectured to qualitatively explain values of observed ranges considerably different from those involving full momentum transfer. Indeed, we find that invariably when the observed values of ranges fall below the full momentum values they can be quantitatively explained with kinematics for the appropriate Q-optimum transfer mechanism along the lines outlined above. In a recent study the evidence[12] for massive transfer involving the complement of an α particle with projectiles ranging from ^{10}B to ^{20}Ne on rare earth targets has been found in α-γ coincidence studies. These examples raise a number of interesting questions such as the following: (i) Why is transfer involving α-particle complements preferred? (ii) Does the presence of this mechanism have something to do with α-cluster configurations in the projectile, or is it only a manifestation of the relatively high stability against breakup of α particles produced in encounters involving heavy ions? (iii) Is this process a forerunner of a more basic and generally present mechanism which involves emission of pre-equilibrium-like α particles from the fusing projectile plus target system, as, for example, appears to have been observed in reactions induced by heavier ions?[13] If not, how can one distinguish one from the other?

The third proposed mechanism involving nonsequential breakup of ^{6}Li into an α particle and a deuteron in the field of a target nucleus with subsequent capture of one of the fragments by the same nucleus is energetically and kinematically similar in its effects on the recoil ranges as the transfer reaction discussed above. First, the noncaptured fragments have the same energy as the outgoing particle in the Q-optimum transfer reaction.[14] Second, the breakup process is also forward peaked and so the outgoing fragment can take away a large amount of the incident momentum. Finally, the nuclei and the excitations at which they are produced following fragment capture by the target nucleus are the same as those produced in the transfer reaction. Therefore, the predicted behavior of the recoil ranges with the ^{6}Li energy for various product nuclei will also be the same in the two cases. Indeed, from the observed character of the recoil ranges there is no way to distinguish one process from the other unless one can make an independent case that the breakup followed by fragment capture is not very likely on some other grounds.

The fourth mechanism, in which high energy α particles are preferentially emitted in a forward direction from the fusing projectile plus target system prior to equilibration, can also lead to the carrying away of much of the incident momentum. The kinematics and energetics of this process may also be not very different from the analogous transfer reaction. But it is hard to see how preequilibrium α emission could ensue prior to preequilibrium nucleon emission which only shows up in significant strength above 70-MeV bombarding energy, unless one postulates that such α emission becomes significant immediately beyond the one α-evaporation peak in the excitation functions.

It is obvious from the discussion presented above that the observed behavior of recoil ranges can be understood in a straightforward manner in terms of the transfer mechanism in which the complement of the α particle for a given projectile is transferred around an optimum Q value. However, further work is needed to answer some of the questions raised in this connection and before one can sort out relative contribution of other processes with similar kinematic characteristics.

B. Comparison with the fusion-evaporation model

In terms of the discussion presented in the last section it is clear that the dominant mechanism for reactions induced by ^{6}Li in the energy range of 10 to 100 MeV is fusion of the projectile and the target nucleus followed by decay of the resulting compound nucleus by statistical evaporation. We have attempted to compare the observed cross section with those predicted by such a model. The calculations were performed with the computer code ALICE[3] using the parameters listed in Table VII. For a representative set of product nuclei the comparisons are depicted in Fig. 8. Qualitatively, the model is able to reproduce the observed shapes, including the double humps, which indeed arise from evaporation of one or two α particles as discussed before. Quantitatively, the magnitudes of the calculated cross section are, except for a few cases, within a factor of 2, and often closer than that, to the observed cross sections over the entire energy range. Given the approximations inherent in the code, especially the limited treatment of the angular momentum dependent effects and neglect of the contributions from nonfusion processes, the agreement is as good as could be expected. By changing the values of the parameters it is possible to get a better account of the observed cross section as a function of the ^{6}Li energy for a given product nucleus or for a broader range of product nuclei at a given energy, but always at a noticeable deterioration for other nuclei and/or other energies. Overall these comparisons confirm rather quantitatively that fusion evaporation is the dominant mechanism.

Another perspective about the mechanism can be obtained by examining the mass distribution shown

in Fig. 6. Here the solid bars represent the predictions by ALICE and the histogram is based upon the observed cross sections. Except for the fact that the predicted cross sections for nuclei with mass 5 or 6 nucleon mass units less than that of the compound nucleus are considerably smaller that the observed values, the overall character of the observed mass distribution is well reproduced by the model. The predicted valley in the vicinity of 5–6 nucleons removed is expected to be filled to some extent by the contributions from transfer processes which make major contributions to the production of nuclei close to the target.

The average number of nucleons removed from the compound nucleus, as observed and predicted by ALICE, are shown in Fig. 7 as a function of the excitation energy of the compound nucleus. At lower energies noticeably lower predicted values may again be signaling the neglect of transfer contributions, which would enhance the production of nuclei closer to the target mass above what is produced by evaporation alone. At higher energies the effect of pre-equilibrium nucleon emission is expected to reduce the average number of emitted nucleons, since pre-equilibrium nucleons carry out noticeably more energy than evaporation nucleons.

C. The total and the fusion cross section

The total observed reaction cross sections over the energy range of this study are compared with those predicted by the parabolic model[15] (curve A), the classical geometric model (curve B), and the optical model[16] (curve C) in Fig. 5. It is obvious that the total observed cross section is a large fraction of the theoretically expected reaction cross section over the entire energy range. The difference between the observed and the optical model cross sections could mostly be due to the contribution of undetected processes which leave the stable product nuclei in their ground states.

Subtracting from the observed cross section the contributions estimated for transfer reactions and for pre-equilibrium nucleon emission (based upon the exponential tails in the excitation functions), we obtain a reasonable estimate for the fusion cross section in the ^{6}Li energy range of 60–80 MeV of 1.3 ± 0.2 b. This represents 0.65 ± 0.10 of the optical model reaction cross sections in the above energy range. This fraction should be compared with the corresponding values of 0.68 and 0.53 obtained[17] for the ^{12}C + Ni system with ^{12}C energies of 98 and 180 MeV, respectively, and with 0.72 obtained for the ^{12}C + Cu system at 98-MeV ^{12}C energy. The similarity in these values for ^{6}Li and ^{12}C projectiles implies that above the same fraction of the reaction cross section leads to fusion in both cases, i.e., ^{6}Li may not be all that different from other light heavy ions in the overall character of its interactions for comparable energy in MeV/nucleon.

IV. SUMMARY AND CONCLUSIONS

From the qualitative and quantitative features of the measured cross sections for a large fraction of the total number of nuclei produced in ^{6}Li induced reactions in the 10- to 100-MeV energy range, and from the recoil ranges of many of the radioactive product nuclei, as presented in this report, we have shown that (a) the dominant reaction mechanism accounting for 80% of the observed cross section is the fusion-evaporation process, (b) recoil range measurements are a very sensitive tool for identifying the presence and determining the quantitative contribution of processes that transfer less than the full incident momentum, (c) a significant contribution, about 300 mb, is made by transfer reactions, especially of the (^{6}Li, α) type, (d) the theoretical predictions of the fusion-evaporation model using the code ALICE agree quite well with the gross features and magnitudes of the observed cross sections, and (e) the fusion cross sections for the ^{6}Li projectile and for other light heavy ions appear to make up a comparable fraction of their respective reaction cross section, implying that ^{6}Li is behaving quite like other light heavy ions in this respect. This study also raises some questions pertaining to the nature and the role of the emission of pre-equilibrium-like α particles which need further study if they are to be answered in an unambiguous way.

ACKNOWLEDGMENTS

The authors are indebted to Professor M. Blann for many helpful discussions and suggestions and to Professor G. Emery for a critical reading of the manuscript. They are also appreciative of the competent help of the IUCF technical staff in many stages of this work. This investigation would not have been possible without patient assistance of Mr. B. Lozowski in preparing numerous targets employed in this work. Two of us (J. J. and H. K.) wish to thank the IUCF management for financial support during our stay in Bloomington. This work was partly supported under the operating grant for IUCF from the National Science Foundation.

*Permanent address: I. N. R., Swierk, Poland.
†Present address: Dept. of Physics, UCLA, Los Angeles, California 90024.

[1]M. Blann, F. M. Lanzafame, and R. A. Piscitelli, Phys. Rev. 133, B700 (1964).
[2]C. K. Cline, Nucl. Phys. A174, 73 (1971).
[3]Evaporation code ALICE; M. Blann, University of Rochester Reports Nos. UR-NSRL-159 and COO-3494-34, 1977 (unpublished).
[4]L. C. Northcliffe and R. F. Schilling, Nucl. Data Tables A7, 233 (1970).
[5]Indiana University Cyclotron Facility Report No. 78-01, 1978 (unpublished).
[6]W. W. Bowman and K. W. MacMurdo, At. Data Nucl. Data Tables 13, 89 (1974).
[7]L. Winsberg and J. M. Alexander, Phys. Rev. 121, 518 (1961).
[8]J. M. Alexander and L. Winsberg, Phys. Rev. 121, 529 (1961).
[9]J. Lindhard and M. Scharff, Phys. Rev. 124, 128 (1961).
[10]Francoise Hubert, thesis presented at l'Université de Bordeaux I, 1973 (unpublished).
[11]H. Delagrange, A. Fleury, F. Hubert, and G. N. Simonoff, Phys. Lett. 37B, 355 (1971).
[12]D. R. Zolnowski, H. Yamada, S. E. Cala, A. C. Kahler, and T. T. Sugihara, Phys. Rev. Lett. 41, 92 (1978).
[13]L. Westerberg, D. G. Sarantites, D. C. Hensley, R. A. Dayras, M. L. Halbert, and J. H. Barker, Phys. Rev. C 18, 796 (1978).
[14]P. J. Siemens, J. P. Bondorf, D. H. E. Gross, and F. Dickmann, Phys. Lett. 36B, 24 (1971).
[15]T. D. Thomas, Phys. Rev. 116, 703 (1959).
[16]P. Schwandt, Elastic-Scattering Analysis Code SNOOPY5, IUCF Report No. 75-1, 1975 (unpublished).
[17]J. B. Natowitz, E. T. Chulick, and M. N. Namboodiri, Phys. Rev. C 6, 2133 (1972).
[18]P. Schwandt *et al.*, Indiana University Cyclotron Facility technical and scientific report, 1978, (unpublished), p. 85.